

phenotype, the *Grid2* open reading frame (ORF) was amplified from cDNA prepared from the cerebellum. As shown in Figure 3B, the *Grid2* ORF was approximately 1 kb shorter in the mutant mice than in the WT mice. In addition, western blotting for GRID2 revealed that this protein was absent from the mutant cerebellum (Figure 3C).

Direct sequencing of the mutant ORF suggested that the region from exon 3 to exon 8 might be deleted, which is the longest deletion reported in *Grid2* mutant mice [31]. Chromosome walking (Figure 3D) identified the break points 110 kb upstream from exon 3 and 30 kb downstream from exon 8, which yielded a truncated GRID2 protein similar to that in the *Grid2^{trp/trp}*, *Grid2^{ho8J/ho8J}*, and *Grid2^{ho13J/ho13J}* mutants, but with different flanking peptides (Figure 3E). Our laboratory code for mutant mouse lines is Htake, thus the mutant allele is named *Grid2^{Htake}*.

2.4. Altered Sensitivity to NMDA in Cultured Granule Cells of *Grid2^{Htake/Htake}* Mice

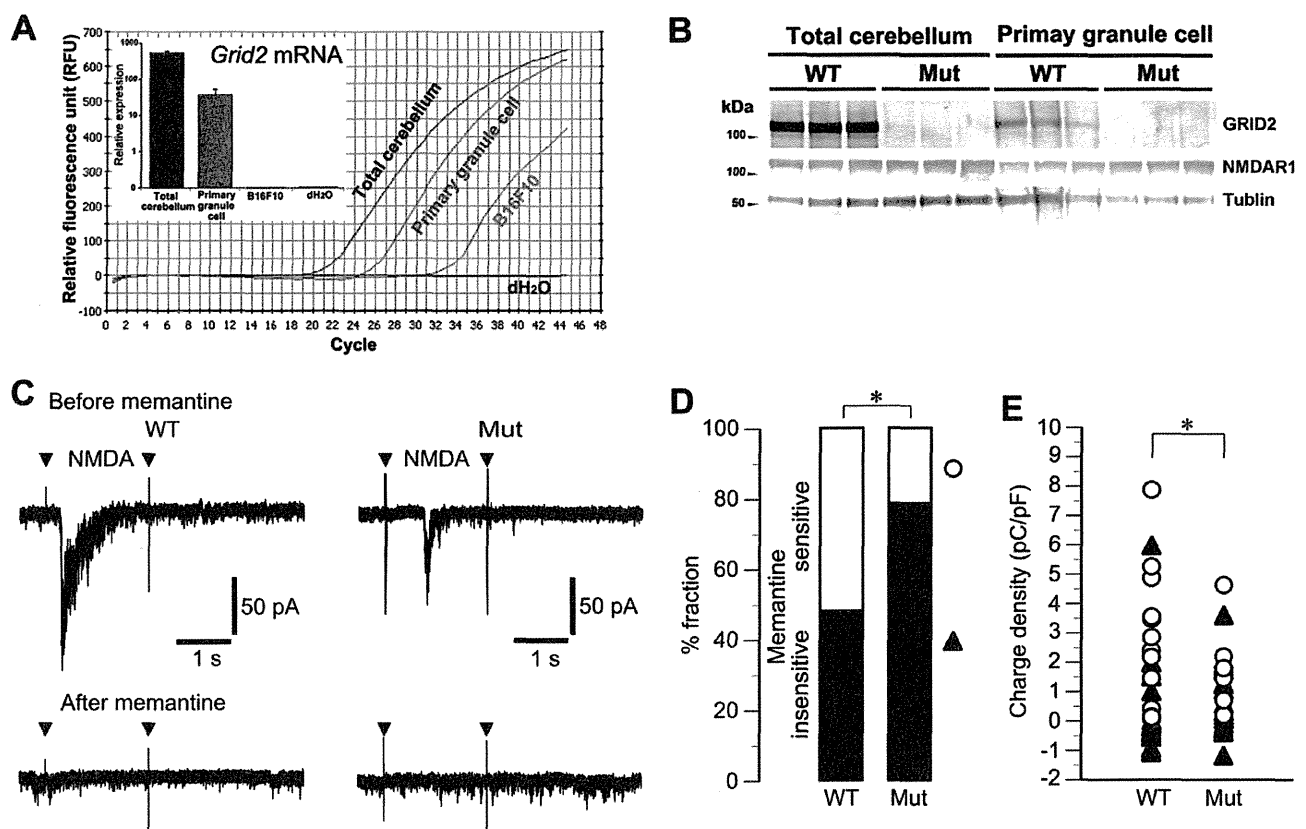
GRID2 is highly expressed in Purkinje cells, and disruption of GRID2 signaling impairs Purkinje cell functions. However, little or no expression of functional NMDA receptors in Purkinje cells of the adult cerebellum has been reported [32]. Thus, it is possible that *Grid2* gene deletion influences cerebellar function by affecting NMDA receptors on granule cells. We examined whether *Grid2^{Htake/Htake}* mice possessed memantine-sensitive NMDA receptors on cerebellar granule cells, using granule cell-enriched (Purkinje cell-free) primary cultures from P2 mice. Quantitative PCR (Figure 4A) and western blot analyses (Figure 4B) showed that cultured granule cells expressed low, but detectable, levels of *Grid2* mRNA and GRID2 protein. No significant difference in NMDAR1 protein level was observed between the cultures derived from normal and *Grid2^{Htake/Htake}* mice, which was consistent with the result of mRNA (microarray) analyses (Supplementary Table S1).

We have to note, however, that no significant interaction between GRID2 protein and NMDAR1 protein in the total cerebella or cultured granule cell lysate was observed (Supplementary Figure S2), despite the presence of PKC gamma binding to GRID2 protein [33].

Next, we monitored NMDA-induced currents in cultured granule cells using a whole-cell voltage-clamp technique. At cell densities as low as 1.25 million cells/mL and a holding potential of -90 mV, granule cells from both WT and mutant mice showed no baseline activity (Figure 4C). In the absence of memantine (before memantine), NMDA ($20 \mu\text{M}$, 2 s) induced inward currents that were larger in WT cells than in mutant cells. Furthermore, NMDA-induced currents were reduced in the presence of memantine (after memantine: $10 \mu\text{M}$, 30 s). However, the magnitude of the memantine-dependent suppression of the NMDA-induced currents varied in the individual cells.

To accurately categorize the memantine-sensitive NMDA-induced currents, we divided the cells into two categories based on the ability of memantine to reduce the charge density of NMDA-induced currents by more than 75%. According to this classification, 51.9% of WT cells and only 21.4% of mutant cells were categorized as memantine-sensitive (Figure 4D). Moreover, the classification (only open circles) revealed that the values of charge density from the mutant cells fell into a lower range, which produced a significant difference in the variance of the charge density between the WT and mutant groups (Figure 4E). These results suggest that mutant mice might possess a poor variation of NMDA receptor with reduced function on their granule cell population.

Figure 4. NMDA-responsiveness of cultured cerebellar granule cells. **(A)** The raw data for quantitative PCR analyses and normalized levels (inset: $n = 4$) of *Grid2* mRNA are indicated. Total RNA was prepared from total cerebellum, 2-week-cultured cerebellar granule cells from neonates (P2), B16F10 melanoma cells (non-neuronal negative control); **(B)** Western blotting was performed using WT and *Grid2*^{Htake/Htake} (Mut) total cerebella or cultured granule cells. There is no significant difference in NMDAR1 protein level; **(C)** Whole-cell current responses of cultured granule cells derived from WT and Mut mice to local application of NMDA (20 μ M, 2 s) before and after treatment with memantine (10 μ M, 30 s). Representative currents recorded from single WT and Mut cells. Arrowheads indicate artifacts due to the opening and closure of the electromagnetic valve controlling delivery of NMDA-containing saline; **(D)** The examined cells were categorized into two groups by memantine susceptibility, and their populations are represented as % fractions. When more than 75% of NMDA-induced inward current was suppressed by memantine, the cells were categorized into the memantine-sensitive group (white area). Cells that experienced reduced inward current suppression after memantine treatment, or no significant inward current were categorized into the memantine-insensitive group (black area). * $p = 0.0178$, likelihood ratio test (WT, $n = 27$; Mut, $n = 28$); **(E)** Distribution of the total charge density of NMDA-induced inward currents. Open circles (white) and closed triangles (black) indicate the data from cells categorized as D. The magnitude of the total data (white and black) was not significantly different between the WT and mutant cells (medians, 1.01 and 0.64 pC/pF, respectively). However, in a comparison of the data from the memantine-sensitive cells (white), there was a significant difference in variance between the WT and mutant cells (* $p = 0.0120$, Brown-Forsythe test).



2.5. Mice Treated with Memantine and AMPA Were Unable to Walk Smoothly

GRID2 deficiency results in dysregulation of AMPA receptors [34,35]. To examine whether impaired AMPA receptor functions affected memantine susceptibility, mice were treated with memantine simultaneously with the AMPA receptor agonist AMPA or the antagonist DNQX [36], and the movements of these mice were monitored (Figure 5A). The mice treated with AMPA (20 mg/kg) walked slowly and sometimes crouched on the floor. However, mice treated with both memantine (10 mg/kg) and AMPA had increased activity and did not stop walking. In addition to these abnormal behaviors, the mice walked with a mild staggering gait and sometimes slipped (roll-over: Figure 5B, Supplementary Movie 4). These combined effects of memantine on mouse behavior were not observed when memantine was administered with DNQX (10 mg/kg), although the mice treated with DNQX were also sometimes crouched. Moreover, in the *Grid2^{Htake/Htake}* mice, co-treatment with AMPA and a low dose of memantine (5 mg/kg) caused more evident balance impairment than memantine treatment alone (Supplementary Figure S3), suggesting that GRID2 deficiency may augment the synergistic action of AMPA and memantine. The effect of AMPA co-treatment could not be evaluated with a higher dose of memantine (10 mg/kg) because the maximal effect was induced by this dose of memantine.

Figure 5. Effect of AMPA receptor modulators on memantine action in WT mice. **(A)** Monitoring of walking mice (12-week-old WT male, $n = 6$) after memantine treatment (10 mg/kg) combined with AMPA (20 mg/kg) or the AMPA receptor antagonist DNQX (10 mg/kg). Ten minutes after the treatments, the walking distance for 5 min was expressed as the mean and SD, * $p < 0.05$ vs. the other conditions (unpaired t -test; $p < 0.0001$ for overall differences, one-way ANOVA); **(B)** Number of rollovers in 5 min was counted. NO indicates that rollover was not observed. $n = 6$ for Control and AMPA + memantine and $n = 3$ for the other conditions. The occurrence of rollover was significantly different between AMPA + memantine and the other conditions ($p < 0.05$, Fisher's exact test); **(C)** OKRs measured in female WT mice with sequential injections of the control saline, AMPA (10 mg/kg), or DNQX (5 mg/kg) and memantine (5 mg/kg). A set of traces indicates representative responses of individual mice. Dotted line, the movement of the stimulus screen; **(D)** Graph shows the mean and \pm SD of OKR gain ($n = 3$ for each condition). p value (without a bracket, one-tailed unpaired t -test; with brackets, paired t -test) is indicated when significance was observed.

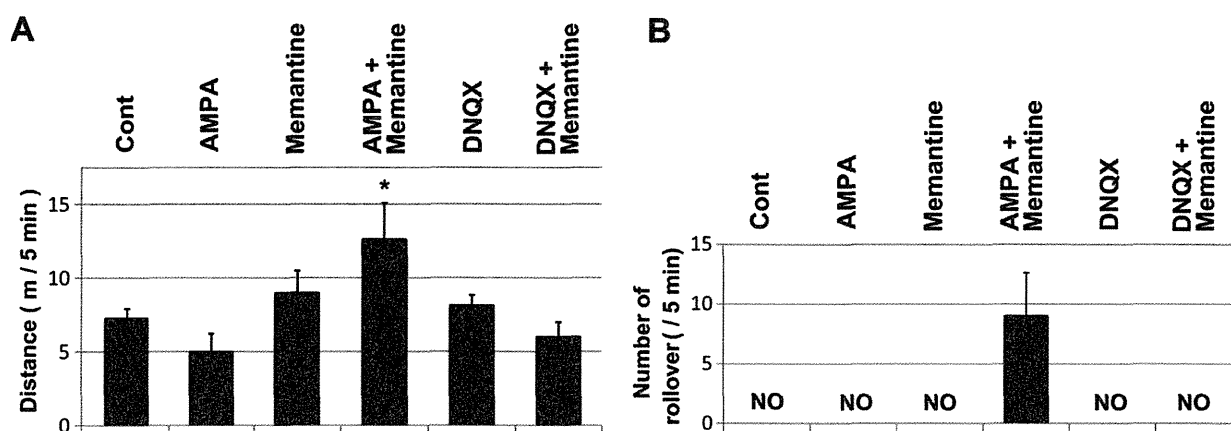
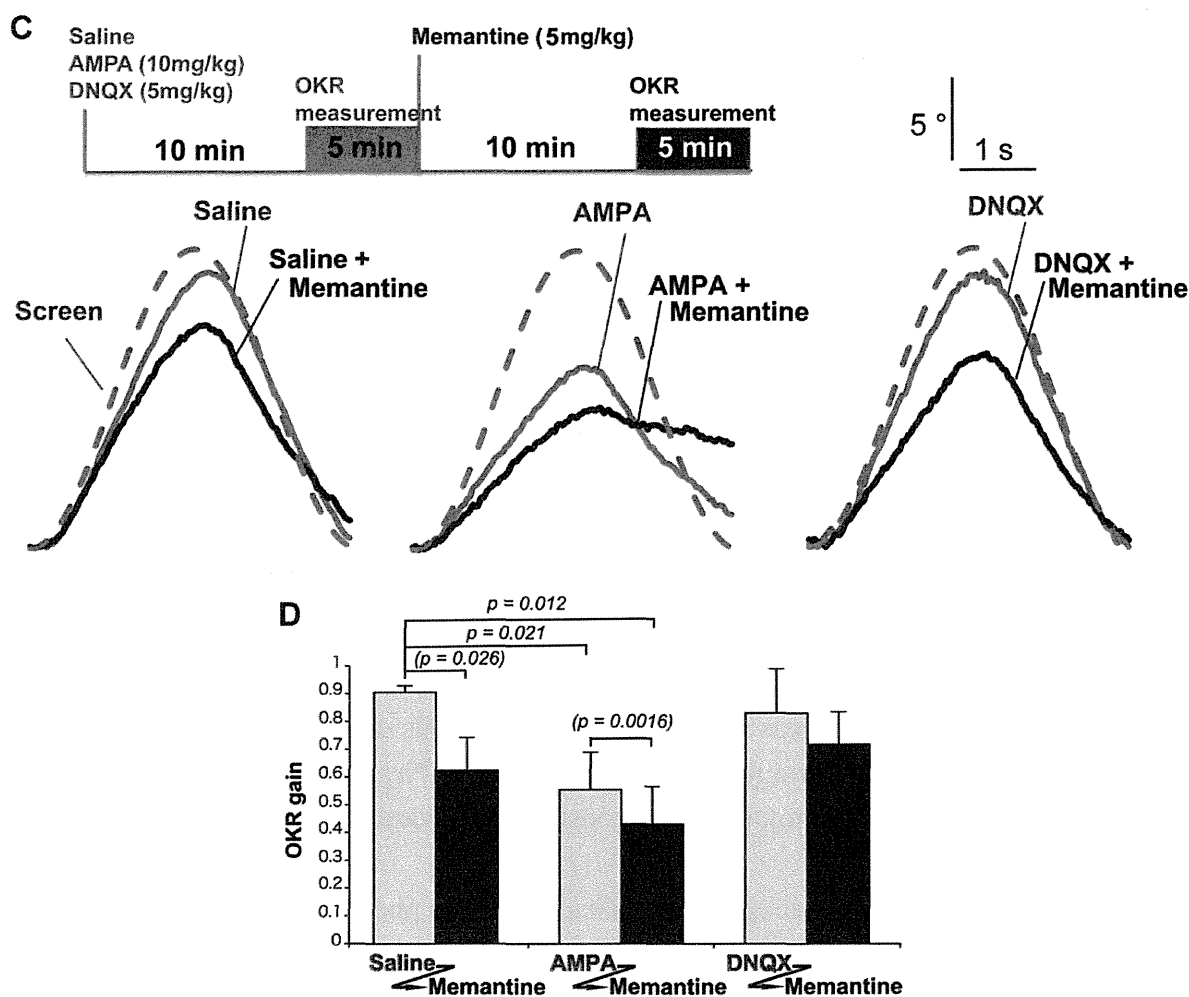


Figure 5. Cont.



Finally, the OKR was monitored after co-treatment with memantine and AMPA or DNQX (Figure 5C). Mice were first treated with AMPA, DNQX, or saline, and the OKR was subsequently monitored for 5 min (because some mice closed their eyes after treatment with higher doses, AMPA (10 mg/kg) and DNQX (5 mg/kg) were used for OKR measurement). To evaluate synergies between memantine and AMPA receptor modulators, the mice were further treated with a low dose of memantine (5 mg/kg), and again subjected to OKR measurements for another 5 min. AMPA significantly impaired the OKR, and the combined treatment with memantine further impaired the OKR (Figure 5D). These effects were not observed in mice co-treated with memantine and DNQX.

3. Discussion

Here, we report cross-talk between GRID2 signaling and memantine in mice, which may, in part, account for the adverse effects of memantine in patients with individual differences in congenital or acquired genetic factors, such as GRID2.

Major phenotypes have been identified in GRID2 mutant mice, including impaired motor coordination, learning, and memory. GRID2 is located on the postsynaptic membrane of Purkinje cells and binds to cerebellin precursor protein 1 (CBLN1) and neurexin 1 beta (NRXN1b) [7,8] on the parallel fibers of granule cells [7,37]. On the other hand, the memantine target, NMDA receptors, are also

expressed on the developing [38] and adult [39] cerebellar granule cells. Furthermore, contrary to the neurotoxic effects of glutamate, NMDA receptors were found to promote the survival of cultured Purkinje [40] and granule cells [41,42]. However, double-KO mice with disrupted *Nr2A* and *Nr2C* genes (encoding two major NMDA receptor subunits in the adult mice cerebellum) demonstrate a mild impairment in motor coordination, but they do not exhibit an ataxic phenotype [43]. This observation suggests that NMDA receptors and GRID2 functions may not be directly linked [44].

Thus, in the present study, pharmaco-behavioral approaches failed to identify *Grid2* as a candidate for the cause of the observed phenotypes. Unexpectedly, our efforts resulted in the observation of new phenotypes in our *Grid2* deficient mice, which appeared as enhanced memantine susceptibility, which was likely mediated by dysfunctional NMDA receptors [1,2,45]. OKR measurements in *Grid2^{Htake/Htake}* mice revealed impaired basal cerebellar functions in eye movement, which was also mimicked by memantine treatment. Dizziness has been reported as a major adverse effect of memantine treatment in humans [6,46]. The cerebellar flocculus is thought to be responsible for the early stage formation of OKR adaptation and its memory [47,48].

The *Grid2* gene is located in a hot spot of genomic deletions [31], and a number of mutant lines with defects in this gene have been identified. In addition to naturally occurring mutants, targeted disruption and knock-in mutations of *Grid2* have been reported [30,49,50]. In contrast to these loss-of-function mutations, *Grid2^{Lc}* (*Lurcher*) [51] was identified as a spontaneous dominant mutation characterized by cerebellar ataxia and atrophy of Purkinje and granule cells [30]. Physiological studies of *Grid2^{Lc/+}* mice have shown that the *Grid2^{Lc}* mutation produces constitutive inward Ca^{2+}/Na^{+} currents that induce cell death [52].

The importance of the genetic background on *Grid2^{Lc/+}* mice phenotypes was also reported [47,53]. In congenic *Grid2^{Lc/+}* mice, almost 99.99% of those on a C57BL/6 genetic background lost Purkinje cells, whereas no Purkinje cell loss was observed in *Grid2^{Lc/+}* mice on a 93% C57BL/6 genetic background, indicating that phenotypes in *Grid2^{Lc/+}* mice are highly dependent on their genetic backgrounds. Interestingly, abnormal eye-movement and impaired motor-coordination were only observed in 93% of C57BL/6 background-*Grid2^{Lc/+}* mice possessing Purkinje cells, but not in 99.99% of C57BL/6 background-*Grid2^{Lc/+}* mice without Purkinje cells [47], suggesting that gain of GRID2 signaling is also a cause of motor deficits in the presence of Purkinje cells. In contrast to *Grid2^{Lc/+}* mice, we noticed during gene mapping that memantine-induced balance impairment was observed in *Grid2^{Htake/Htake}* mice irrespective of their genetic backgrounds (mixed B6 and C3 backgrounds). This is also the case for random eye movements commonly observed in different *Grid2*-deleted mice with different genetic backgrounds, *Grid2*-KO in C57BL/6 and *Grid2^{ho-15J/15J}* on a C3HJ background [17], suggested that memantine-induced balance impairment may occur in other *Grid2* deficient mice irrespective of their genetic backgrounds.

How does the *Grid2^{Htake}* deletion enhance the actions of memantine? GRID2 regulates long-term depression (LTD) at synapses between immature parallel fibers and Purkinje cells by inducing AMPA receptor endocytosis [34,35]. D-Serine is an endogenous ligand for GRID2 and one of the factors that induce LTD [9]. Developing mice that express GRID2 with a disrupted D-serine binding site show impaired motor coordination and learning, suggesting the importance of LTD for motor regulation. On the other hand, NMDA receptor activation requires the removal of Mg^{2+} block, which occurs when the membrane potential increases through activation of non-NMDA receptors including AMPA receptors [4].

Cooperative signal-transmission from cerebellar mossy fiber-granule cells to Purkinje cells mediated by NMDA and AMPA receptors has been shown in both Mg^{2+} block dependent and independent manners [54]. We observed that co-treatment with memantine and AMPA impaired gait and OKR in wild type mice, suggesting that dysregulation of AMPA receptor function in *Grid2* deficient mice may cause the enhanced memantine susceptibility. This may be implicated in the decreased number of memantine-sensitive NMDA-responsible granule cells in *Grid2*^{Htake/Htake} mice.

Whilst mapping the gene responsible for the ataxic phenotype, we observed new phenotypes in *Grid2* deficient mice, which were latent balance defects, and OKR impairments. These deficits were also mimicked by memantine with AMPA in the impaired WT mice. Because, recently, the wide distributions of *Grid2* mRNA and GRID2 protein were reported in the adult rodent brain [55], the phenotypes in *Grid2*^{Htake/Htake} mice could be ascribed to not only attenuated NMDA receptor responsiveness in a subset of granule cells but also other cellular mechanisms.

When granule cells are collectively activated *in vivo*, glutamate spilt over from parallel fiber-Purkinje cell synapses stimulate adjacent interneurons (volume transmission), which in turn exert inhibition of Purkinje cells [44,56–58] crucial for normal motor coordination [59]. The GRID2 mutation may reduce NMDA receptor-mediated excitation of granule cells, and this might decrease the volume transmission and Purkinje cell inhibition via interneurons. Moreover, cerebellar interneurons (basket, stellate, and Golgi cells) also express functional NMDA receptors at their presynaptic membrane [44,56–58] and these receptors could be affected by the change of GRID2 signaling. Taken as a whole, the present study using a naturally occurring *Grid2* deleted mouse line may lead to a better understanding of NMDA, AMPA, and GRID2 receptors. Further studies are required to elucidate the precise mechanisms underlying GRID2 signaling.

4. Experimental Section

4.1. Animals

C57BL/6J (B6) and C3H/HeN (C3) from SLC Japan (Shizuoka, JAPAN) were used for the maintenance of the *Grid2*^{Htake/Htake} mouse line and for IVF for microsatellite analyses, respectively. IVF was performed following a standard method [60] using human tubal fluid medium (Ark Resource, Kumamoto, Japan). The *Grid2* mutant mice, *Grid2*^{Htake/Htake} (formal name is *Grid2*^{ho-Htake}/Nibio), were supplied by the JCRB Laboratory Animal Resource Bank at the National Institute of Biomedical Innovation. The experimental mouse protocols were approved by the Ethics Committee at the National Institute of Biomedical Innovation (assigned No. DS-23-35), and by the University of Toyama's Committee on Animal Experiments (assigned No. A2012eng-8) for animal welfare. For microarray analyses, cerebella were dissected after anesthesia of mice with isoflurane (WAKO Pure Chemicals, Osaka, JAPAN). The animals were maintained under standard light (08:00–20:00) and temperature conditions (23 °C, 50% humidity).

4.2. Reagents

Microsatellite markers were used to identify the chromosomal region responsible for the ataxic phenotype, (D6Mit86, 1.18 cM; D6Mit351, 22.94 cM; D6Mit384, 27.38 cM; D6Mit243, 32.2 cM 7;

D6Mit29, 37.75 cM; D6Mit102, 42.11 cM; D6Mit149, 48.93 cM; D6Mit200, 89.28 cM). To map the end points of the *Grid2* deletion, we used following primers: m*Grid2* intron 2H F 5'-GCT ACT TTG GTA CAA GTG GAC A and m*Grid2* intron 2H R 5'-GAC AAG TTG CTC TCT GTA TCT; m*Grid2* Intron 2I F 5'-CAT GCT CAC ATC AAA ATA CAT CAA and m*Grid2* Intron 2I R 5'-TGT AAT TGA GGAA AAT ACA TAA T. Other primers used in Figure 3D were prepared with reference to [31]. To identify the *Grid2* deletion in *Grid2^{Htake/Htake}* mice, we used the following primers for PCR amplification: m*Grid2* Intron 2HIF 5'-TGG ATC CTT CTA CGT GCA AC, m*Grid2* Intron 8YF2 5'-GGA CCA CAC TGA GGT TCG AAA GA, and m*Grid2* Intron 8YR 5'-ATC TCT TGG CAT GCA TTA GAC. The mutant allele of *Grid2^{Htake}* produces a PCR band corresponding to a product of approximately 600 bp, and that for the WT allele is approximately 400 bp.

GRID2 antibody was obtained from Santa Cruz Biotechnology (Santa Cruz, CA, USA). Antibodies for NMDAR1 and tubulin were obtained from Cell Signaling Technology (Boston, MA, USA). Memantine, AMPA, DNQX, MK-801, nitrazepam, donepezil, and ondansetron were purchased from WAKO Pure Chemicals; ifenprodil, Ro25-6981, DL-AP7, felbamate, and loperamide were obtained from Sigma-Aldrich (St. Louis, MO, USA).

4.3. mRNA Analyses

Total RNA was prepared from the cerebellar hemispheres of 12-week-old mice (male and female) using the EZ1-RNA purification kit (Qiagen, Venlo Park, The Netherlands). For microarray analyses, GeneChip Mouse Genome 430A (Affymetrix, Santa Clara, CA, USA) was used, and differences in transcript levels were calculated with Partek (Partek Inc., St. Louis, MO, USA). The original data files (CEL-files) were deposited in the Gene Expression Omnibus (GEO) repository and assigned the GEO accession numbers: GSM1334015, GSM1334016, and GSM1334017 for normal mice, and GSM1334018, GSM1334019, and GSM1334020 for mutant mice. PCR primers for real-time PCR were as follows: m*Grid2* F, 5'-AAC ACG CTA CAT GGA CTA CTC-3' and m*Grid2* R, 5'-GAA GCA CTG TGC CAG CAA TG-3'; m*Gapdh* F, 5'-ACT CAC GGC AAA TTC AAC GG-3' and m*Gapdh* R, 5'-GAC TCC ACG ACA TAC TGA GC-3'. To amplify the *Grid2* ORF, primers are m*Grid2* F2 (5ATG): 5'-ATG GAA GTT TTC CCC TTG CTC TTG T and m*Grid2* R (3Stop): 5'-TCA TAT GGA CGT GCC TCG GTC GGG GTC A were used.

4.4. Measurements of Walking Distance and the OKR

Male mice (12–14 weeks old) were placed in a rectangular box (25 cm × 40 cm), and their head position was tracked for 5 min using ANY-maze software (Brain Science Idea, Osaka, Japan). Each mouse was monitored three times, and the longest distance recorded was used in the data analysis.

The OKR was measured in adult mice using previously described methods [28], which are depicted in Supplementary Figure S1. Briefly, the mice were anesthetized with isoflurane (2%) and a stainless steel screw was glued to the skull. The mice were then habituated to the experimental conditions for 2 days before the measurement. Ten minutes before the measurement were made, mice were administered a saline (8 mL/kg) injection with or without memantine (10 mg/kg) intraperitoneally. The mouse was then mounted on a stereotaxic apparatus and exposed to continuous sinusoidal horizontal oscillations (17°, 0.25 Hz) of a cylindrical checkerboard-patterned screen (diameter, 65 cm; single

square, 1.8×1.8 cm; brightness, ~ 30 lx). Right eye movement was captured at 30 Hz with an infrared camera. For each image frame, we used a machine vision system to estimate the pupil azimuth from the location of the pupil center. The OKR was expressed on a time plot of the relative pupil azimuth for each round of screen oscillation, with the pupil azimuth at the beginning of backward eye movement set to 0° . An OKR gain was defined as the ratio of the maximal relative pupil azimuth change to that of the screen (17°).

4.5. Cell Culture and Electrophysiology

Granule cell-enriched cultures were prepared as previously described [61]. Briefly, 2-day-old (P2) mutant or WT mice were anesthetized by cooling and then sacrificed by decapitation. The cerebella were dissociated with trypsin, plated on poly-L-ornithine-coated plastic dishes (Becton Dickinson, Franklin Lakes, NJ, USA) at 1.25 million cells/mL, and maintained in low-serum, nutrient-supplemented Dulbecco's Modified Eagle Medium/F-12 (Life Technologies; 5% CO₂, 37 °C) for 12 days.

Ruptured-patch whole-cell recordings were performed on cultured granule cells. The pipette solution contained 134 mM potassium D-gluconic acid, 7.6 mM KCl, 9 mM KOH, 10 mM NaCl, 1.2 mM MgCl₂, 4 mM ATP magnesium salt, 10 mM HEPES, and 0.5 mM EGTA (pH 7.3). The culture dish was perfused at a rate of 1.4 mL/min with 145 mM NaCl, 5 mM KCl, 2 mM CaCl₂, 10 mM HEPES, 10 mM D-glucose, and 10 μ M glycine (pH 7.4). Current signals were recorded using an EPC-8 amplifier (holding potential, -90 mV; cut-off frequency, 5 kHz; sampling rate, 20 kHz; HEKA, Lambrecht/Pfalz, Germany) controlled by Patchmaster software (version, 2.35; HEKA). The command potentials were corrected for a liquid junction potential between the pipette and bath solutions. Electronic capacitance cancellation and series resistance compensation were not used. The series resistance (33.2 ± 5.1 M Ω , $n = 55$) and membrane capacitance were estimated from the amplitude and time constant of the capacitive current evoked by a 10 mV voltage jump. The bath solution containing 20 μ M NMDA or 10 μ M memantine was locally applied to the cell through a theta tube under the control of gravity and electromagnetic valves (VM8, ALA Scientific Instruments, Farmingdale, NY, USA). The magnitude of an NMDA-induced current was quantified as the inward current charge over a 2 s NMDA application normalized to the membrane capacitance (charge density). The background charge was estimated from a 0.5 s pre-application period and subtracted from the charge density.

4.6. Statistical Analyses

Data from each group were characterized by the mean \pm SD, unless otherwise stated. Data from biochemical assays were examined with one-way ANOVA followed by unpaired two-tailed *t*-tests to detect statistically significant differences. All the statistical examinations were performed using JMP software (versions 9.0.2 and 10.0.1, SAS Institute, Cary, NC, USA).

Acknowledgments

We thank Junko Morita for her technical assistance and Takayoshi Imazawa for their kind advice. We thank Sebnem Kesaf and Ryuichi Shigemoto for their advice on performing OKR measurements.

This study was supported by Grants-in-Aid for Scientific Research from the Ministry of Education, Culture, Sports, Science, and Technology, Japan (25670155, 23500384, 23500384); the grant from the Ministry of Health, Labor, and Welfare (2013–2017, 2014–2016); Scientific Research on Innovative Areas, a MEXT Grant-in-Aid Project 2012–2013; Strategic Research Foundation at Private Universities (2013–2017); the grant from the Human Science Foundation (2012–2013); and a grant from the Uehara Memorial Foundation.

Author Contributions

A.K., A.F., T.Y., Y.N., Y.H., T.S., Y.I., M.K., O.S., S.A, H.R., A.K., L.P.T, M.S., T.F., H.T. performed experiments. K.K., Y.N., H.K., K.M., T.N., J.M. T.T., H.T. analyzed data. T.T., H.T. wrote the manuscript.

Conflicts of Interest

No conflicts of interest, financial or otherwise, are declared by the author(s).

References

1. Sonkusare, S.K.; Kaul, C.L.; Ramarao, P. Dementia of Alzheimer's disease and other neurodegenerative disorders—Memantine, a new hope. *Pharmacol. Res.* **2005**, *51*, 1–17.
2. Lipton, S.A. Paradigm shift in neuroprotection by NMDA receptor blockade: Memantine and beyond. *Nat. Rev. Drug Discov.* **2006**, *5*, 160–170.
3. Szczurowska, E.; Mares, P. NMDA and AMPA receptors: Development and status epilepticus. *Physiol. Res.* **2013**, *62* (Suppl. 1), S21–S38.
4. Kupper, J.; Ascher, P.; Neyton, J. Probing the pore region of recombinant N-methyl-D-aspartate channels using external and internal magnesium block. *Proc. Natl. Acad. Sci. USA* **1996**, *93*, 8648–8653.
5. Wong, E.H.; Kemp, J.A.; Priestley, T.; Knight, A.R.; Woodruff, G.N.; Iversen, L.L. The anticonvulsant MK-801 is a potent N-methyl-D-aspartate antagonist. *Proc. Natl. Acad. Sci. USA* **1986**, *83*, 7104–7108.
6. Hansen, R.A.; Gartlehner, G.; Lohr, K.N.; Kaufer, D.I. Functional outcomes of drug treatment in Alzheimer's disease: A systematic review and meta-analysis. *Drugs Aging* **2007**, *24*, 155–167.
7. Uemura, T.; Lee, S.J.; Yasumura, M.; Takeuchi, T.; Yoshida, T.; Ra, M.; Taguchi, R.; Sakimura, K.; Mishina, M. Trans-synaptic interaction of GluRdelta2 and Neurexin through Cbln1 mediates synapse formation in the cerebellum. *Cell* **2010**, *141*, 1068–1079.
8. Matsuda, K.; Miura, E.; Miyazaki, T.; Kakegawa, W.; Emi, K.; Narumi, S.; Fukazawa, Y.; Ito-Ishida, A.; Kondo, T.; Shigemoto, R.; *et al.* Cbln1 is a ligand for an orphan glutamate receptor delta2, a bidirectional synapse organizer. *Science* **2010**, *328*, 363–368.
9. Kakegawa, W.; Miyoshi, Y.; Hamase, K.; Matsuda, S.; Matsuda, K.; Kohda, K.; Emi, K.; Motohashi, J.; Konno, R.; Zaitzu, K.; *et al.* D-Serine regulates cerebellar LTD and motor coordination through the delta2 glutamate receptor. *Nat. Neurosci.* **2011**, *14*, 603–611.

10. Jardon, B.; Bonaventure, N. N-Methyl-D-aspartate antagonists suppress the development of frog symmetric monocular optokinetic nystagmus observed after unilateral visual deprivation. *Brain Res. Dev. Brain Res.* **1992**, *67*, 67–73.
11. Godaux, E.; Cheron, G.; Mettens, P. Ketamine induces failure of the oculomotor neural integrator in the cat. *Neurosci. Lett.* **1990**, *116*, 162–167.
12. Mettens, P.; Cheron, G.; Godaux, E. NMDA receptors are involved in temporal integration in the oculomotor system of the cat. *Neuroreport* **1994**, *5*, 1333–1336.
13. Huang, Y.J.; Lin, C.H.; Lane, H.Y.; Tsai, G.E. NMDA Neurotransmission Dysfunction in Behavioral and Psychological Symptoms of Alzheimer’s Disease. *Curr. Neuropharmacol.* **2012**, *10*, 272–285.
14. Puangthong, U.; Hsiung, G.Y. Critical appraisal of the long-term impact of memantine in treatment of moderate to severe Alzheimer’s disease. *Neuropsychiatr. Dis. Treat.* **2009**, *5*, 553–561.
15. Utine, G.E.; Haliloglu, G.; Salanci, B.; Cetinkaya, A.; Kiper, P.O.; Alanay, Y.; Aktas, D.; Boduroglu, K.; Alikasifoglu, M. A Homozygous Deletion in GRID2 Causes a Human Phenotype With Cerebellar Ataxia and Atrophy. *J. Child Neurol.* **2013**, *28*, 926–932.
16. Maier, A.; Klopocki, E.; Horn, D.; Tzschach, A.; Holm, T.; Meyer, R.; Meyer, T. *De novo* partial deletion in GRID2 presenting with complicated spastic paraplegia. *Muscle Nerve* **2014**, *49*, 289–292.
17. Hills, L.B.; Masri, A.; Konno, K.; Kakegawa, W.; Lam, A.T.; Lim-Melia, E.; Chandy, N.; Hill, R.S.; Partlow, J.N.; Al-Saffar, M.; *et al.* Deletions in GRID2 lead to a recessive syndrome of cerebellar ataxia and tonic upgaze in humans. *Neurology* **2013**, *81*, 1378–1386.
18. Van Schil, K.; Meire, F.; Karlstetter, M.; Bauwens, M.; Verdin, H.; Coppieters, F.; Scheiffert, E.; van Nechel, C.; Langmann, T.; Deconinck, N.; *et al.* Early-onset autosomal recessive cerebellar ataxia associated with retinal dystrophy: New human hotfoot phenotype caused by homozygous GRID2 deletion. *Genet. Med.* **2014**, doi:10.1038/gim.2014.95.
19. Uebi, T.; Itoh, Y.; Hatano, O.; Kumagai, A.; Sanosaka, M.; Sasaki, T.; Sasagawa, S.; Doi, J.; Tatsumi, K.; Mitamura, K.; *et al.* Involvement of SIK3 in glucose and lipid homeostasis in mice. *PLOS ONE* **2012**, *7*, e37803.
20. Hemmings, H.C., Jr.; Yan, W.; Westphalen, R.I.; Ryan, T.A. The general anesthetic isoflurane depresses synaptic vesicle exocytosis. *Mol. Pharmacol.* **2005**, *67*, 1591–1599.
21. Rammes, G.; Danysz, W.; Parsons, C.G. Pharmacodynamics of memantine: An update. *Curr. Neuropharmacol.* **2008**, *6*, 55–78.
22. Seeman, P.; Caruso, C.; Lasaga, M. Memantine agonist action at dopamine D2High receptors. *Synapse* **2008**, *62*, 149–153.
23. Lee, J.W.; Park, H.J.; Choi, J.; Park, S.J.; Kang, H.; Kim, E.G. Comparison of ramosetron’s and ondansetron’s preventive anti-emetic effects in highly susceptible patients undergoing abdominal hysterectomy. *Korean J. Anesthesiol.* **2011**, *61*, 488–492.
24. Khojasteh, A.; Sartiano, G.; Tapazoglou, E.; Lester, E.; Gandara, D.; Bernard, S.; Finn, A. Ondansetron for the prevention of emesis induced by high-dose cisplatin. A multi-center dose-response study. *Cancer* **1990**, *66*, 1101–1105.
25. Jayadev, S.; Bird, T.D. Hereditary ataxias: Overview. *Genet. Med.* **2013**, *15*, 673–683.

26. Requena, T.; Espinosa-Sanchez, J.M.; Lopez-Escamez, J.A. Genetics of dizziness: Cerebellar and vestibular disorders. *Curr. Opin. Neurol.* **2014**, *27*, 98–104.
27. Rosini, F.; Federighi, P.; Pretegiani, E.; Piu, P.; Leigh, R.J.; Serra, A.; Federico, A.; Rufa, A. Ocular-motor profile and effects of memantine in a familial form of adult cerebellar ataxia with slow saccades and square wave saccadic intrusions. *PLOS ONE* **2013**, *8*, e69522.
28. Shirai, Y.; Asano, K.; Takegoshi, Y.; Uchiyama, S.; Nonobe, Y.; Tabata, T. A simple machine vision-driven system for measuring optokinetic reflex in small animals. *J. Physiol. Sci.* **2013**, *63*, 395–399.
29. Shutoh, F.; Ohki, M.; Kitazawa, H.; Itohara, S.; Nagao, S. Memory trace of motor learning shifts transsynaptically from cerebellar cortex to nuclei for consolidation. *Neuroscience* **2006**, *139*, 767–777.
30. Zuo, J.; de Jager, P.L.; Takahashi, K.A.; Jiang, W.; Linden, D.J.; Heintz, N. Neurodegeneration in Lurcher mice caused by mutation in delta2 glutamate receptor gene. *Nature* **1997**, *388*, 769–773.
31. Wang, Y.; Matsuda, S.; Drews, V.; Torashima, T.; Meisler, M.H.; Yuzaki, M. A hot spot for hotfoot mutations in the gene encoding the delta2 glutamate receptor. *Eur. J. Neurosci.* **2003**, *17*, 1581–1590.
32. Cull-Candy, S.G.; Wyllie, D.J. Glutamate-receptor channels in mammalian glial cells. *Ann. N. Y. Acad. Sci.* **1991**, *633*, 458–474.
33. Kato, A.S.; Knierman, M.D.; Siuda, E.R.; Isaac, J.T.; Nisenbaum, E.S.; Brecht, D.S. Glutamate receptor delta2 associates with metabotropic glutamate receptor 1 (mGluR1), protein kinase Cgamma, and canonical transient receptor potential 3 and regulates mGluR1-mediated synaptic transmission in cerebellar Purkinje neurons. *J. Neurosci.* **2012**, *32*, 15296–15308.
34. Hirai, H.; Launey, T.; Mikawa, S.; Torashima, T.; Yanagihara, D.; Kasaura, T.; Miyamoto, A.; Yuzaki, M. New role of delta2-glutamate receptors in AMPA receptor trafficking and cerebellar function. *Nat. Neurosci.* **2003**, *6*, 869–876.
35. Yamasaki, M.; Miyazaki, T.; Azechi, H.; Abe, M.; Natsume, R.; Hagiwara, T.; Aiba, A.; Mishina, M.; Sakimura, K.; Watanabe, M. Glutamate receptor delta2 is essential for input pathway-dependent regulation of synaptic AMPAR contents in cerebellar Purkinje cells. *J. Neurosci.* **2011**, *31*, 3362–3374.
36. Honore, T.; Davies, S.N.; Drejer, J.; Fletcher, E.J.; Jacobsen, P.; Lodge, D.; Nielsen, F.E. Quinoxalinediones: Potent competitive non-NMDA glutamate receptor antagonists. *Science* **1988**, *241*, 701–703.
37. Kakegawa, W.; Miyazaki, T.; Kohda, K.; Matsuda, K.; Emi, K.; Motohashi, J.; Watanabe, M.; Yuzaki, M. The N-terminal domain of GluD2 (GluRdelta2) recruits presynaptic terminals and regulates synaptogenesis in the cerebellum *in vivo*. *J. Neurosci.* **2009**, *29*, 5738–5748.
38. Rabacchi, S.; Bailly, Y.; Delhaye-Bouchaud, N.; Mariani, J. Involvement of the N-methyl-D-aspartate (NMDA) receptor in synapse elimination during cerebellar development. *Science* **1992**, *256*, 1823–1825.
39. Garthwaite, J.; Brodbelt, A.R. Synaptic activation of N-methyl-D-aspartate and non-N-methyl-D-aspartate receptors in the mossy fibre pathway in adult and immature rat cerebellar slices. *Neuroscience* **1989**, *29*, 401–412.

40. Yuzaki, M.; Forrest, D.; Verselis, L.M.; Sun, S.C.; Curran, T.; Connor, J.A. Functional NMDA receptors are transiently active and support the survival of Purkinje cells in culture. *J. Neurosci.* **1996**, *16*, 4651–4661.
41. Balazs, R.; Jorgensen, O.S.; Hack, N. N-Methyl-D-aspartate promotes the survival of cerebellar granule cells in culture. *Neuroscience* **1988**, *27*, 437–451.
42. Ortega, F.; Perez-Sen, R.; Morente, V.; Delicado, E.G.; Miras-Portugal, M.T. P2X7, NMDA and BDNF receptors converge on GSK3 phosphorylation and cooperate to promote survival in cerebellar granule neurons. *Cell. Mol. Life Sci.* **2010**, *67*, 1723–1733.
43. Kadotani, H.; Hirano, T.; Masugi, M.; Nakamura, K.; Nakao, K.; Katsuki, M.; Nakanishi, S. Motor discoordination results from combined gene disruption of the NMDA receptor NR2A and NR2C subunits, but not from single disruption of the NR2A or NR2C subunit. *J. Neurosci.* **1996**, *16*, 7859–7867.
44. Marmolino, D.; Manto, M. Past, present and future therapeutics for cerebellar ataxias. *Curr. Neuropharmacol.* **2010**, *8*, 41–61.
45. Bormann, J. Memantine is a potent blocker of N-methyl-D-aspartate (NMDA) receptor channels. *Eur. J. Pharmacol.* **1989**, *166*, 591–592.
46. Strupp, M.; Brandt, T. Current treatment of vestibular, ocular motor disorders and nystagmus. *Ther. Adv. Neurol. Disord.* **2009**, *2*, 223–239.
47. Yoshida, T.; Katoh, A.; Ohtsuki, G.; Mishina, M.; Hirano, T. Oscillating Purkinje neuron activity causing involuntary eye movement in a mutant mouse deficient in the glutamate receptor delta2 subunit. *J. Neurosci.* **2004**, *24*, 2440–2448.
48. Faulstich, M.; van Alphen, A.M.; Luo, C.; du Lac, S.; De Zeeuw, C.I. Oculomotor plasticity during vestibular compensation does not depend on cerebellar LTD. *J. Neurophysiol.* **2006**, *96*, 1187–1195.
49. Gordon, J.W.; Uehlinger, J.; Dayani, N.; Talansky, B.E.; Gordon, M.; Rudomen, G.S.; Neumann, P.E. Analysis of the hotfoot (ho) locus by creation of an insertional mutation in a transgenic mouse. *Dev. Biol.* **1990**, *137*, 349–358.
50. Kashiwabuchi, N.; Ikeda, K.; Araki, K.; Hirano, T.; Shibuki, K.; Takayama, C.; Inoue, Y.; Kutsuwada, T.; Yagi, T.; Kang, Y.; *et al.* Impairment of motor coordination, Purkinje cell synapse formation, and cerebellar long-term depression in GluR delta 2 mutant mice. *Cell* **1995**, *81*, 245–252.
51. Wilson, D.B. Brain abnormalities in the lurcher (Lc) mutant mouse. *Experientia* **1975**, *31*, 220–221.
52. Nishiyama, J.; Matsuda, K.; Kakegawa, W.; Yamada, N.; Motohashi, J.; Mizushima, N.; Yuzaki, M. Reevaluation of neurodegeneration in lurcher mice: Constitutive ion fluxes cause cell death with, not by, autophagy. *J. Neurosci.* **2010**, *30*, 2177–2187.
53. Cendelin, J.; Tuma, J.; Korelusova, I.; Vozeh, F. The effect of genetic background on behavioral manifestation of Grid2(Lc) mutation. *Behav. Brain Res.* **2014**, *271*, 218–227.
54. Schwartz, E.J.; Rothman, J.S.; Dugue, G.P.; Diana, M.; Rousseau, C.; Silver, R.A.; Dieudonne, S. NMDA receptors with incomplete Mg(2)(+) block enable low-frequency transmission through the cerebellar cortex. *J. Neurosci.* **2012**, *32*, 6878–6893.
55. Hepp, R.; Hay, Y.A.; Aguado, C.; Lujan, R.; Dauphinot, L.; Potier, M.C.; Nomura, S.; Poirel, O.; El Mestikawy, S.; Lambolez, B.; *et al.* Glutamate receptors of the delta family are widely expressed in the adult brain. *Brain Struct. Funct.* **2014**, doi:10.1007/s00429-014-0827-4.

56. Glitsch, M.D. Calcium influx through N-methyl-D-aspartate receptors triggers GABA release at interneuron-Purkinje cell synapse in rat cerebellum. *Neuroscience* **2008**, *151*, 403–409.
57. Liu, S.J. Biphasic modulation of GABA release from stellate cells by glutamatergic receptor subtypes. *J. Neurophysiol.* **2007**, *98*, 550–556.
58. Duguid, I.C.; Smart, T.G. Retrograde activation of presynaptic NMDA receptors enhances GABA release at cerebellar interneuron-Purkinje cell synapses. *Nat. Neurosci.* **2004**, *7*, 525–533.
59. Hirano, T.; Watanabe, D.; Kawaguchi, S.Y.; Pastan, I.; Nakanishi, S. Roles of inhibitory interneurons in the cerebellar cortex. *Ann. N. Y. Acad. Sci.* **2002**, *978*, 405–412.
60. Whittingham, D.G. Fertilization of mouse eggs *in vitro*. *Nature* **1968**, *220*, 592–593.
61. Tabata, T.; Sawada, S.; Araki, K.; Bono, Y.; Furuya, S.; Kano, M. A reliable method for culture of dissociated mouse cerebellar cells enriched for Purkinje neurons. *J. Neurosci. Methods* **2000**, *104*, 45–53.

© 2014 by the authors; licensee MDPI, Basel, Switzerland. This article is an open access article distributed under the terms and conditions of the Creative Commons Attribution license (<http://creativecommons.org/licenses/by/4.0/>).

Salt-inducible kinase 3 deficiency exacerbates lipopolysaccharide-induced endotoxin shock accompanied by increased levels of pro-inflammatory molecules in mice

Masato Sanosaka,¹ Minoru Fujimoto,² Tomoharu Ohkawara,² Takahiro Nagatake,³ Yumi Itoh,¹ Mai Kagawa,¹ Ayako Kumagai,¹ Hiroyuki Fuchino,⁴ Jun Kunisawa,³ Tetsuji Naka² and Hiroshi

Takemori¹

¹Laboratory of Cell Signalling and Metabolic Disease, National Institute of Biomedical Innovation, Ibaraki, Osaka, ²Laboratory of Immune Signalling, National Institute of Biomedical Innovation, Ibaraki, Osaka, ³Laboratory of Vaccine Materials, National Institute of Biomedical Innovation, Ibaraki, Osaka, and ⁴Research Centre for Medicinal Plant Resources, National Institute of Biomedical Innovation, Tsukuba, Ibaraki, Japan

doi:10.1111/imm.12445

Received 25 July 2014; revised 14 January 2015; accepted 20 January 2015.

Correspondence: M. Sanosaka and H. Takemori, Laboratory of Cell Signalling and Metabolic Disease, National Institute of Biomedical Innovation (NIBIO), 7-6-8, Asagi, Saito, Ibaraki, Osaka 567-0085, Japan. Emails: m-sanosaka@nibio.go.jp and takemori@nibio.go.jp

Senior author: Xxxx

Summary

Macrophages play important roles in the innate immune system during infection and systemic inflammation. When bacterial lipopolysaccharide (LPS) binds to Toll-like receptor 4 on macrophages, several signalling cascades co-operatively up-regulate gene expression of inflammatory molecules. The present study aimed to examine whether salt-inducible kinase [SIK, a member of the AMP-activated protein kinase (AMPK) family] could contribute to the regulation of immune signal not only in cultured macrophages, but also *in vivo*. LPS up-regulated SIK3 expression in murine RAW264.7 macrophages and exogenously over-expressed SIK3 negatively regulated the expression of inflammatory molecules [interleukin-6 (IL-6), nitric oxide (NO) and IL-12p40] in RAW264.7 macrophages. Conversely, these inflammatory molecule levels were up-regulated in SIK3-deficient thioglycollate-elicited peritoneal macrophages (TEPM), despite no impairment of the classical signalling cascades. Forced expression of SIK3 in SIK3-deficient TEPM suppressed the levels of the above-mentioned inflammatory molecules. LPS injection (10 mg/kg) led to the death of all SIK3-knockout (KO) mice within 48 hr after treatment, whereas only one mouse died in the SIK1-KO ($n = 8$), SIK2-KO ($n = 9$) and wild-type ($n = 8$ or 9) groups. In addition, SIK3-KO bone marrow transplantation increased LPS sensitivity of the recipient wild-type mice, which was accompanied by an increased level of circulating IL-6. These results suggest that SIK3 is a unique negative regulator that suppresses inflammatory molecule gene expression in LPS-stimulated macrophages.


Keywords: AMP-activated protein kinase; endotoxin shock; interleukin-12p40; interleukin-1 β ; interleukin-6; inducible nitric oxide synthase; macrophage; salt-inducible kinases; tumour necrosis factor- α

Introduction

Macrophages play a critical role in the innate immune system during infection and systemic inflammation.¹ They produce pro-inflammatory cytokines such as tumour necrosis factor- α (TNF- α), interleukin-6 (IL-6) and IL-12 through recognition of bacterial components via Toll-like receptors (TLRs). Lipopolysaccharide (LPS; a cell-wall component of Gram-negative bacteria) is the ligand for TLR4.^{2,3} When LPS binds to TLR4, its adaptor protein, the myeloid differentiation factor (MyD)88, recruits and activates IL-1 receptor-associated kinase

family proteins,^{4,5} which is followed by the activation of the transforming growth factor- β -activated kinase 1 (TAK1). The active TAK then transmits the signal through different pathways such as those involving the I κ B kinase (IKK) family (I κ B α -nuclear factor- κ B) and the mitogen-activated protein kinases [MAPKs: extracellular signal-regulated kinase (ERK), p38, and c-Jun N-terminal kinase (JNK)]. TAK1 phosphorylates MAPK kinases (MKKs) and induces the activation of MAPKs.⁶⁻⁸

These MyD88-dependent cascades are initiated at an immediate early phase. In contrast, interferon- β -producing cascades such as those involving the interferon

Dispatch: 10.2.15	CE: Nancy
No. of pages: 11	PE: Amul
WILEY	
12445	Manuscript No.
I M M	Journal Code
	

regulatory factor 3 (IRF3) and the signal transducer and activator of transcription (STAT1) are activated by the MyD88-independent and Toll interleukin receptor-domain-containing adapter-inducing interferon- β -dependent pathways, which contributes to the late activation of nuclear factor- κ B.^{3,4,9–11} The gene expression of nitric oxide (NO) synthase 2 (Nos2 or inducible NOS; iNOS), which produces the inflammatory mediator NO, is also induced by active STAT1.^{12,13}

Macrophages produce not only pro-inflammatory cytokines, but also anti-inflammatory cytokines. Macrophages are classified into two types, according to their pro-inflammatory or anti-inflammatory functions, classically activated macrophages (M1 macrophages) and alternatively activated macrophages (M2 macrophages), respectively. M2 macrophages are further classified into M2a, M2b, M2c, M2d¹⁴ and M2b macrophages (also called regulatory macrophages) and produce anti-inflammatory cytokines such as IL-10.¹⁵

Salt-inducible kinase (SIK) is a member of the AMP-activated protein kinase (AMPK) family and plays a role in the regulation of glucose and lipid metabolism.^{16,17} SIKs regulate the expression of several genes via the cAMP response element-binding protein (CREB) and myocyte enhancer factor 2 (MEF-2) transcription factors. The former is inhibited by SIKs via the phosphorylation-dependent inactivation of CREB-regulated transcription co-activators (CRTC), which are CREB-specific co-activators^{18–20} and the latter is activated via phosphorylation-dependent inactivation of class IIa histone deacetylases (HDAC), which act as co-repressors for MEF-2.^{21,22} Both CRTC and class IIa HDACs are sensitive to the cAMP-protein kinase A and calcineurin (phosphatase) cascades in which protein kinase A inactivates SIKs and calcineurin reactivates CRTC and class IIa HDACs.¹⁹

Recently, SIK inhibitors were reported to polarize macrophages toward the M2b type through IL-10 production in a CRTC3-dependent manner.^{23,24} On the other hand, Yong Kim *et al.*²⁵ reported that SIK1 and SIK3 negatively regulate TLR4-mediated signalling through interruption of the TAK1-binding protein (TAB)2–TNF receptor-associated factor (TRAF)6 complex by the inhibition of ubiquitination-dependent TRAF6 degradation. These reports suggest that SIKs play important roles in the inflammation and innate immune systems in cultured macrophages. However, the involvement of SIKs in inflammation *in vivo*, except for that in liver inflammation, cholestasis and cholelithiasis in SIK3-knockout (KO) mice,²⁶ remains unclear.

Here, we found that SIK3-KO mice, but not SIK1-KO and SIK2-KO mice, were highly sensitive to LPS and that SIK3-deficient macrophages produced increased levels of the inflammatory molecules, iNOS, IL-6 and IL-12p40 without any significant difference in the classical immune cascades. Moreover, adoptive transfer of SIK3-KO-bone

marrow (SIK3-KO-BM) to X-ray-irradiated wild-type (WT) mice also increased LPS sensitivity in these mice.

Materials and methods

Mice

Age- and sex-matched littermates of SIK1-KO (C57BL/6J \times 129 background), SIK2-KO and SIK3-KO (C57BL/6J background) mice described previously^{26–28} were used in this study. For bone marrow transplantation, 8-week-old male C57BL/6J mice (Japan SLC, Hamamatsu, Japan) were used. All animal experiments were conducted according to the institutional ethical guidelines for animal experimentation of the National Institute of Biomedical Innovation (approved as nos. DS20-56, DS24-41 and DS26-86).

Cell culture

The murine RAW264.7 monocytic/macrophage cell line was obtained from the American Type Culture Collection (Manassas, VA). The cells were cultured in RPMI-1640 medium (Wako, Osaka, Japan) supplemented with 10% heat-inactivated fetal bovine serum (FBS) (Life Technologies, Carlsbad, CA). The isolation of mouse thioglycollate-elicited peritoneal macrophages (TEPM) is described elsewhere.²⁹ Briefly, 10- to 16-week-old mice were injected with 2 ml of 4% (w/v) Brewer's thioglycollate medium (BD Biosciences, San Diego, CA). Three or four days after the injection, the mice were killed by cervical dislocation under deep anaesthesia with isoflurane and their peritoneal macrophages were harvested by lavage with ice-cold PBS. The lavage fluid was transferred into polypropylene tubes, centrifuged at 370 g for 10 min, and the peritoneal macrophages were seeded at a density of 5.0×10^5 cells/cm². The non-adherent cells were washed out twice with PBS warmed at 37° and then cultivated in 10% FBS/RPMI-1640.

Real-time quantitative reverse transcription PCR

Total RNA was prepared using the ReliaPrep™ RNA Cell Miniprep System (Promega, Madison, WI), according to the manufacturer's instructions. Complementary DNA was synthesized by reverse transcription (RT) of 1 μ g of total RNA by using the ReverTra Ace® qPCR RT Kit (Toyobo, Osaka, Japan) and used for quantitative PCR. The primers used in this study are listed in the Supporting information (Table S1).

Lentiviral transduction of SIK3 in RAW264.7 cells

The stable RAW264.7 line that over-expressed SIK3 was transduced using the ViraPower™ HiPerform™

Promoterless Gateway[®] Expression System (Life Technologies), according to the manufacturer's protocol. Briefly, the mouse *Sik3* (mSIK3) open reading frame was amplified by PCR with primers containing attB1/2 sequences, and the PCR product was cloned into the pDONR221 plasmid with BP clonase (Life Technologies). The mSIK3 open reading frame and the cytomegalovirus (CMV) promoter that was cloned into the pENTR plasmid were transferred into the plenti6.4-R4R2-DEST plasmid for preparing the lentiviral vector through the LR reaction. pLP1, pLP2, pLP-VSVG and plenti6.4-CMV-mSIK3 or -LacZ (control) were transformed into 293FT cells using the calcium phosphate method.³⁰ After 72 hr of transformation, the supernatant containing lentiviruses was collected and viral particles were purified using the Lenti-X[™] Concentrator (Clontech, Mountain View, CA), according to the manufacturer's protocol. RAW264.7 cells were infected with lentiviruses, and the infected cells were selected by 10 µg/ml blasticidin (Santa Cruz Inc., Santa Cruz, CA) for 10 days.

Adenoviral transduction of SIK3 in thioglycollate-elicited mouse peritoneal macrophages

Adenoviral expression vectors for Lac Z, human SIK3 (hSIK3)-WT, and hSIK3-K37M mutant (kinase inactive form) were previously described.³¹ The amplified adenoviruses were purified using Fast-Trap[®] Virus Purification and Concentration Kit (Millipore, Billerica, MA) according to the manufacturer's protocol. Thioglycollate-elicited mouse peritoneal macrophages isolated from SIK3-KO or WT mice were infected with adenoviruses (at a multiplicity of infection of 250) for 1 hr. After infection, the cells were washed with serum-free RPMI-1640 medium twice and incubated with 5% FBS/RPMI-1640 for 2 days.

Western blotting

The cells were washed three times with ice-cold PBS and lysed with the 1 × SDS buffer (50 mM Tris-HCl, 10% glycerol, 2% SDS; pH 6.8) without bromophenol blue. After measurement of protein concentration using **5** Bicinchoninic acid (BCA) Protein Assay reagents (Thermo Scientific, Waltham, MA), the lysates were diluted with a one-third volume of 3 × SDS buffer supplemented with 10% 2-mercaptoethanol and bromophenol blue and heated at 100° for 5 min. Proteins (5–15 µg) were separated by SDS-PAGE and electrophoretically transferred onto PVDF membranes. The membranes were blocked with the Blocking One solution (Nacalai Tesque, Kyoto, Japan) and incubated with the following antibodies at 4° overnight: anti-SIK3 (1 : 2000; as per the method described earlier³¹), anti- α / β -tubulin (1 : 3000; #2148), anti-phospho-IKK α / β (1 : 1000; #2697), anti-IKK α / β (1 : 2000; sc-7607), anti-phospho-I κ B α (1 : 1000;

#2859), anti-I κ B α (1 : 1000; #4812), anti-phospho-ERK (1 : 2000; #4376), anti-ERK (1 : 2000; #4695), anti-phospho-p38 (1 : 2000; #9215), anti-p38 (1 : 2000; #9212), anti-phospho-JNK (1 : 1000; #9251), anti-JNK (1 : 1000; #9252), anti-iNOS (1 : 500; sc-7271), anti-phospho-(pY701)-STAT1 (1 : 2000; #7649), anti-STAT1 (1 : 3000; #9172), anti-phospho-IRF3 (1 : 1000; #4947), anti-IRF3 (1 : 1000; #4302), or anti- β -actin (1 : 1000; sc-47778). Except for anti-IKK α / β , anti-iNOS, and anti- β -actin antibodies, which were purchased from Santa Cruz Biotechnology, all other antibodies were purchased from Cell Signaling Technology (Danvers, MA). Next, the membranes were incubated with an anti-rabbit horseradish peroxidase-conjugated goat antibody (111-035-144; Jackson ImmunoResearch Laboratory, West Grove, PA) or an anti-mouse horseradish peroxidase-conjugated goat antibody (1 : 10 000; 115-035-166; Jackson ImmunoResearch Laboratory) for 1 hr. The Chemi-Lumi One Super solution (Nacalai Tesque) was used for the detection of immune complexes.

Bone marrow transplantation

Bone marrow cells were prepared from the femur, tibia, humerus and pelvis of WT or SIK3-KO mice. Recipient mice were irradiated with X-ray (7 Gy). The cells (1 × 10⁷ cells/head) were intravenously injected in the tail vein of irradiated recipient mice. Eight weeks after the transplantation, the recipient mice were used for experiments.

LPS-induced endotoxin shock model

Lipopolysaccharide (10 mg/kg body weight; derived from O111 *Escherichia coli*; phenol-extracted, Wako) dissolved in PBS was injected intraperitoneally into 14-week-old mice. Blood was collected from a small cut on the tail, and serum was separated by centrifugation at 1000 g for 10 min, collected into tubes, and stored at -40° until analysis.

Measurement of cytokine production by ELISA

The cytokine levels in media containing LPS-stimulated mouse peritoneal macrophages or RAW264.7 cells were quantified by ELISA with the ELISA MAX[™] Deluxe (BioLegend, San Diego, CA), as per the manufacturer's instructions. The cytokine levels were normalized to those of cellular protein measured by using the BCA Protein Assay Kit (Thermo Scientific).

Measurement of NO production

Griess reagent (0.05% naphthylethylenediamine dihydrochloride, 0.5% sulphonylamide and 2.5% phosphoric

acid) was prepared and stored at 4° in the dark. Media from LPS-stimulated mouse TEPM or RAW264.7 cells were collected into fresh tubes and then mixed with Griess reagent at a 1 : 1 ratio in a 96-well plate. Absorbance was measured spectrophotometrically at 550 nm. Concentration of NO was normalized to the cellular protein concentration measured by using the BCA Protein Assay Kit (Thermo Scientific).

Statistical analyses

For all experiments, data are expressed as mean ± standard error of the mean (SEM), with at least three repeats for each experimental group. Statistical analyses were performed using the Student's *t*-test or two-way analysis of variance followed by Bonferroni's post-tests for the comparison of gene expression and cytokine secretion. The Cox–Mantel test was used to analyse the Kaplan–Meier curve for mouse survival.

Results

Increase in SIK3 mRNA level after LPS treatment in RAW264.7 macrophages

According to recent studies using SIK inhibitors and RNA interference techniques,^{23,25} all SIK isoforms contribute to inflammatory responses in macrophages. However, information regarding the expression of each SIK isoform in macrophages is limited. To measure the expression of SIK family kinases in macrophages, RAW264.7 cells were stimulated with LPS (Fig. 1). Sixteen hours after LPS treatment, the mRNA level of SIK3, but not SIK1 or SIK2, was significantly up-regulated in RAW264.7 macrophages treated with 10, 100 and 1000 ng/ml LPS (Fig. 1a). We also examined the time-dependent change of SIK isoform mRNA levels after LPS (100 ng/ml) stimulation (Fig. 1b). The SIK3 mRNA level hovered at a high level of expression compared with that observed in the control (only medium replacement), from 4 to 16 hr after LPS stimulation. A small, or less, difference in SIK1 or SIK2 mRNA level was observed between LPS stimulation and control (two-way analysis of variance followed by Bonferroni's post-test suggested a significance in SIK2 mRNA at the 4 hr-point).

SIK3 over-expression suppresses inflammatory molecule expression

To examine whether the different level of SIK3 expression affects the levels of pro-inflammatory or anti-inflammatory molecules after LPS stimulation, we prepared mouse SIK3 (mSIK3) over-expressing RAW264.7 macrophages using lentiviruses. Western blotting revealed that SIK3 protein level in mSIK3 over-expressing cells was higher

than that in the control cells (Lac Z) (Fig. 2a). Suppressed mRNA levels of IL-6, iNOS and IL-12p40 were observed after LPS stimulation (Fig. 2b). However, no significant difference in TNF- α and IL-1 β mRNA levels was observed between the control and mSIK3 over-expressing cells. On the other hand, 1 hr after LPS stimulation, IL-10 mRNA levels were also lower in mSIK3 over-expressed RAW264.7 macrophages than in LacZ-control.

SIK3-deficient macrophages produce high levels of inflammatory molecules

Next, we examined the effects of SIK3 deficiency on the levels of inflammatory molecules. Because the RNA interference technique was not successful for SIK3 in our laboratory, we prepared TEPM from SIK3-KO and WT mice. In contrast to the findings in mSIK3 over-expressed RAW264.7 macrophages, after 4 hr of LPS stimulation, the mRNA levels of IL-6, iNOS and IL-12p40 were higher in SIK3-KO TEPM than in WT TEPM (Fig. 3a). In addition, no significant difference was observed in TNF- α or IL-1 β expression levels between SIK3-KO and WT TEPM. These results suggested that the molecules whose expression was regulated by SIK3 are restricted to the secondary genes that were not fully induced at 1 hr after LPS stimulation. On the other hand, IL-10 mRNA level was also higher in SIK3-KO TEPM than in WT TEPM at 1 hr after LPS stimulation, suggesting that the increase in the expression of secondary genes in SIK3-KO TEPM might be out of the control of, or independent of, the IL-10 altered expression.

In addition to mRNA quantification, we measured the production of cytokines (IL-6, TNF- α and IL-10) and NO in SIK3-KO TEPM (Fig. 3b,c). After stimulation with LPS, SIK3-KO TEPM produced higher IL-6 (twofold, Fig. 3b left panel) and NO (3.5-fold, Fig. 3c) levels than WT TEPM. In contrast, TNF- α production in SIK3-KO TEPM was lower than that in WT TEPM (Fig. 3b middle panel). Interleukin-10 production was also slightly, but clearly, higher in SIK3-KO TEPM than in WT TEPM (Fig. 3b right panel). Furthermore, adenovirus-mediated SIK3 reconstitution in the SIK3-KO TEPM lowered IL-6 production to the level observed in WT TEPM (Fig. 3d, e), which was not observed when a kinase-defective SIK3 (K37M mutant) was reconstituted.

The completeness of signalling cascades in the induction of inflammatory molecules was confirmed by Western blotting (Fig. 3f, classified into the primary response). No significant difference was observed in IKK, I κ B α and MAPK phosphorylation levels between WT and SIK3-KO TEPM after LPS stimulation. However, the JNK protein total level was lower in SIK3-KO TEPM than in WT TEPM, but phosphorylated JNK levels did not differ in these macrophages. In addition to these primary

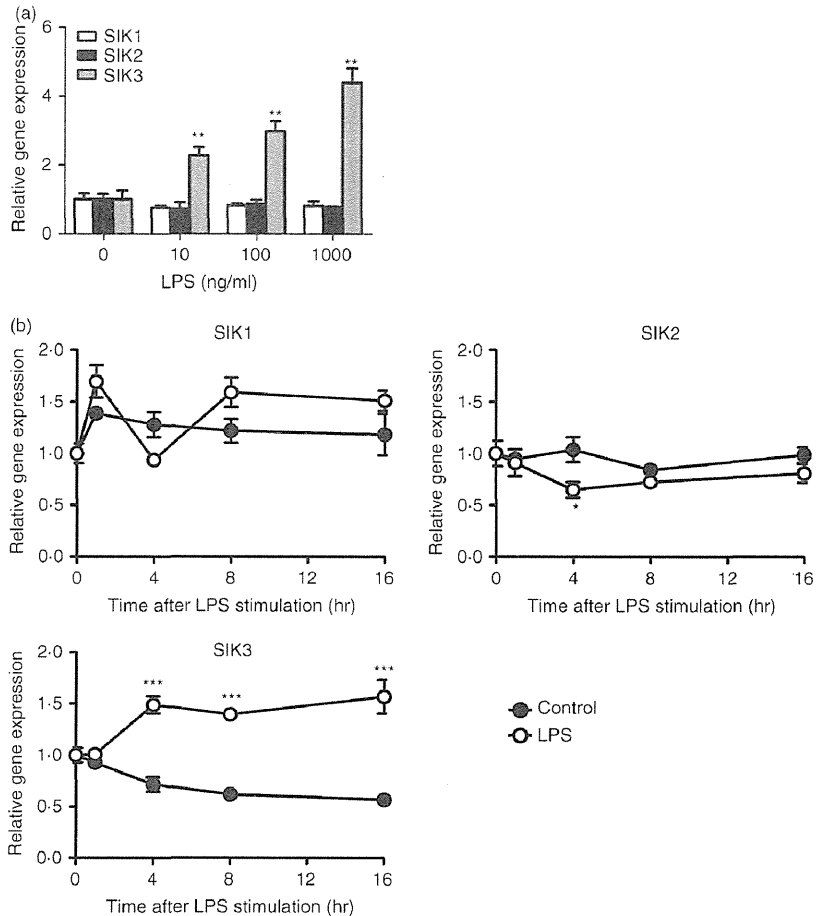


Figure 1. Salt-inducible kinase (SIK) family kinase gene expression levels in RAW264.7 cells after lipopolysaccharide (LPS) treatment. (a) RAW264.7 cells (1.5×10^5 cells/cm²) were stimulated with the indicated dose of LPS for 16 hr. (b) RAW264.7 cells were stimulated with 100 ng/ml LPS and harvested at the indicated time-points. After total RNA isolation, the mRNA levels of SIK1, SIK2 and SIK3 were analysed by quantitative PCR. HPRT₁ was used as an internal control. The data are expressed as mean \pm SEM ($n = 3$). Statistical analyses were performed using the Student's *t*-test (a) or two-way analysis of variance followed by Bonferroni's post-tests (b) for the comparison of gene expression. * $P < 0.05$, ** $P < 0.01$, *** $P < 0.001$.

response cascades, phosphorylation levels of secondary response signal transducers such as IRF3 and STAT1 also did not differ in macrophages (Fig. 3g).

In addition to SIK3-KO TEPM experiments, we prepared TEPM from SIK1-KO and SIK2-KO mice and quantified pro-inflammatory and anti-inflammatory molecule mRNA expression. Notably, IL-10 mRNA level was down-regulated in SIK1-KO macrophages at 1 hr after LPS stimulation (see Supporting information, Fig. S1a), whereas it was up-regulated in SIK2-KO macrophages (Fig. S1b). Although statistical analyses showed some differences in other gene expression levels between WT and SIK1-KO or SIK2-KO TEPM, these differences (especially in the levels of secondary genes) were smaller than those between SIK3-KO TEPM and its control WT TEPM (Fig. 3a).

To argue about the nature of macrophages in SIK3 signalling, we assessed the expression of pro-inflammatory and anti-inflammatory molecules in bone marrow-derived macrophages (BMDM) prepared from WT or SIK3-KO mice (see Supporting information, Fig. S2). Consistent with the results of TEPM, significant differences in IL-6 and iNOS mRNA levels between SIK3-KO and WT BMDM were observed at 4 hr after LPS stimulation.

Furthermore, IL-12p40 mRNA was higher in SIK3-KO BMDM than in WT BMDM. Lower TNF- α levels and higher IL-10 levels in SIK3-KO BMDM than in WT BMDM were observed at 1 hr after LPS stimulation.

SIK3 deficiency exacerbates endotoxin shock in mice

The absence of SIK3 resulted in enhanced mRNA levels of the inflammatory molecules categorized as secondary genes. To examine the importance of SIK3 in the regulation of LPS-induced endotoxin shock *in vivo*, SIK3-KO mice were intraperitoneally injected with 10 mg/kg of LPS (Fig. 4a). All SIK3-KO mice died within 48 hr of LPS injection, whereas only one mouse died in the SIK1-KO, SIK2-KO and control groups (WT, both C57BL/6 and C57BL/6 \times 129 genetic backgrounds). Serum IL-6 levels in WT, SIK1-KO and SIK2-KO mice rapidly increased after LPS treatment, reached a peak at 2–4 hr, and then decreased (Fig. 4b). However, a continuous increase in the serum IL-6 level in SIK3-KO mice was observed until 8 hr after LPS treatment. In all mouse groups, serum TNF- α levels rapidly reached a peak 1 hr after LPS treatment (Fig. 4c). Decreased serum TNF- α level in SIK2-KO and SIK3-KO mice was observed. These

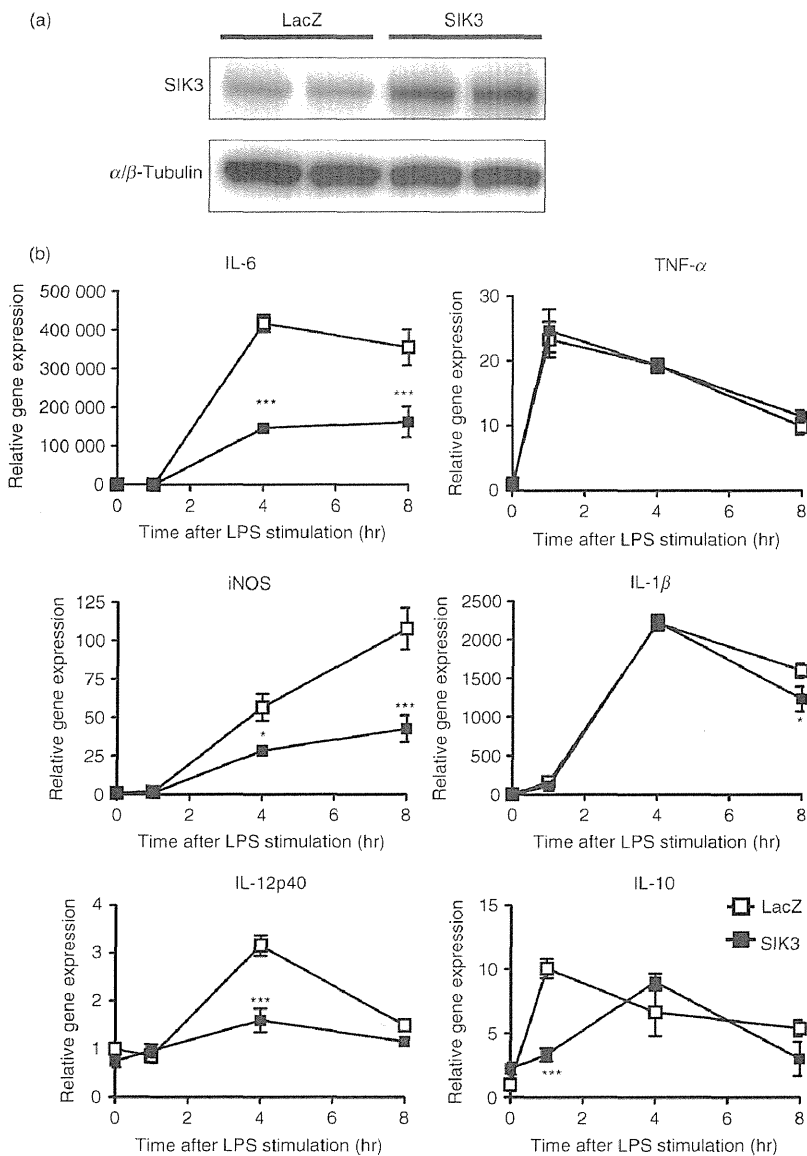


Figure 2. Effect of salt-inducible kinase 3 (SIK3) over-expression on pro-inflammatory molecule mRNA levels in RAW264.7 macrophages. (a) Western blotting confirmed murine SIK3 (mSIK3) protein over-expression in lentiviral-transduced RAW264.7 cells. (b) LacZ (control) and mSIK3 over-expressing RAW264.7 cells were stimulated with lipopolysaccharide (LPS; 100 ng/ml) and the cells were harvested at the indicated time-points. The mRNA levels of pro-inflammatory molecules [interleukin-6 (IL-6), inducible nitric oxide synthase (iNOS), IL-12p40, tumour necrosis factor- α (TNF- α), IL-1 β , and IL-10] were analysed by quantitative PCR. HPRT was used as an internal control. The data are expressed as mean \pm SEM ($n = 3$). Statistical analyses were performed using two-way analysis of variance followed by Bonferroni's post-tests for the comparison of gene expression. * $P < 0.05$, ** $p < 0.01$, *** $p < 0.001$.

results suggest that SIK3 is related to LPS sensitivity *in vivo* and that the dysregulation of secondary inflammatory responses in macrophages is a representative phenotype of SIK3 deficiency.

Transplantation of SIK3-deficient bone marrow increases LPS sensitivity

To confirm whether the increase in LPS sensitivity in SIK3-KO mice was attributed to haematopoietic cells, we prepared bone marrow haematopoietic cells from WT or SIK3-KO mice and adoptively transfer them to X-ray-irradiated WT mice. Reconstitution of SIK3-KO or WT haematopoietic cells was confirmed by PCR using genomic DNA isolated from blood or tail of these recipient mice (Fig. 5a). After LPS treatment, eight out of nine mice that had been reconstituted with SIK3-KO

haematopoietic cells (SIK3-KO-BM mice) died within 4 days (Fig. 5b), whereas only two out of nine mice reconstituted with the control WT haematopoietic cells (WT-BM mice) died. The level of IL-6 production after LPS treatment was also higher in SIK3-KO-BM mice than in WT-BM mice (Fig. 5c), but no significant difference in TNF- α level was observed (Fig. 5d). These results suggested that SIK3-deficient haematopoietic cells, probably macrophages, might contribute to the increased death rate of SIK3-KO mice after LPS treatment.

Discussion

Recent studies with small compounds proposed that SIK family kinases are the signal transducers of the inflammatory response in macrophages through the regulation of CRTC-CREB systems.^{23,24} However, the unified direc-

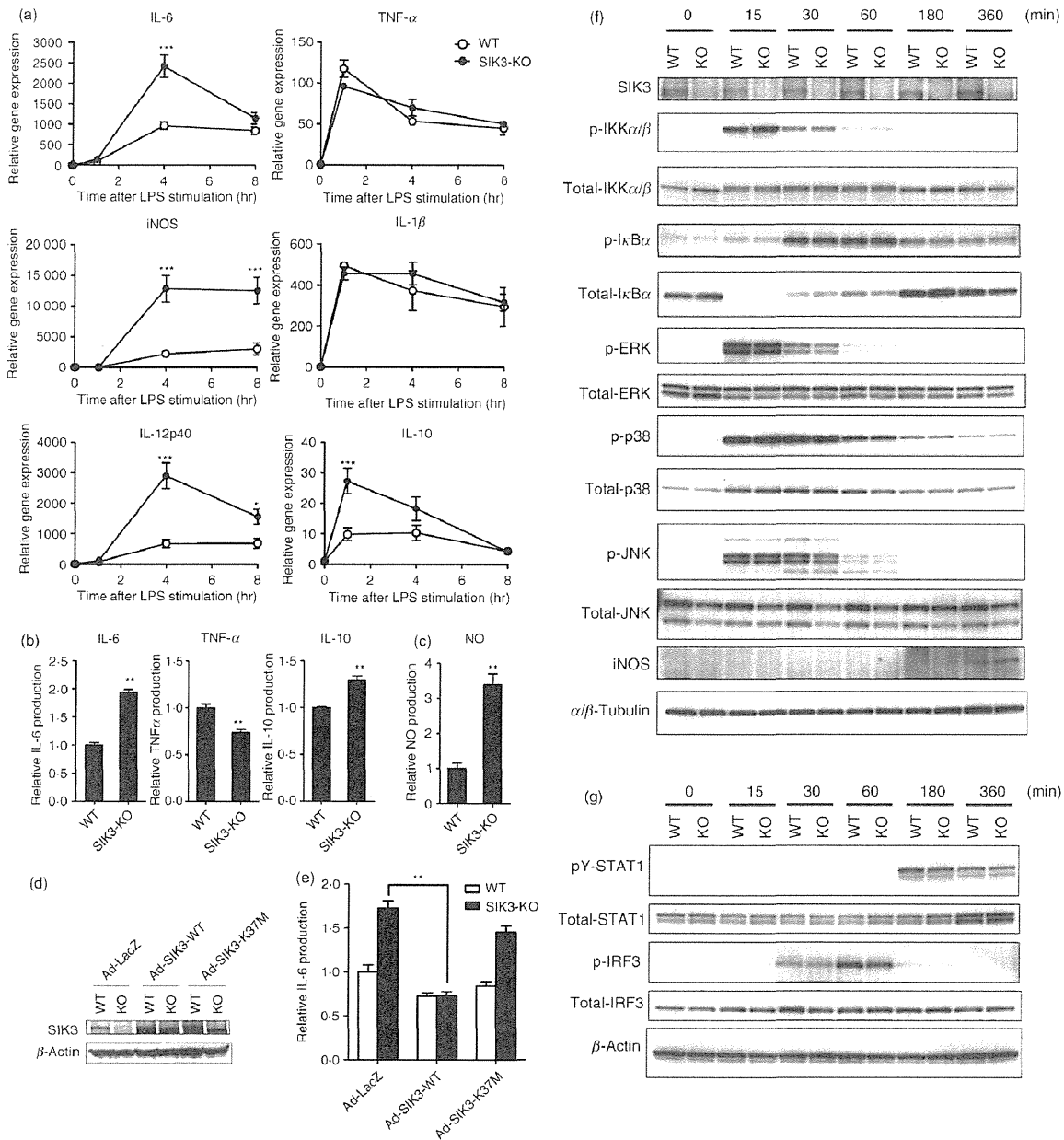


Figure 3. Gene expression and production of pro-inflammatory molecules in salt-inducible kinase 3 (SIK3) -deficient peritoneal macrophages. (a) Thioglycollate-elicited peritoneal macrophages (TEPM) were isolated from SIK3 knockout (-KO) and wild-type (WT) mice and then stimulated with 100 ng/ml lipopolysaccharide (LPS). The cells were then harvested at the indicated time-points for gene expression analyses of pro-inflammatory molecules [interleukin-6 (IL-6), inducible nitric oxide synthase (iNOS), IL-12p40, tumour necrosis factor- α (TNF- α) and IL-1 β]. HPRT was used as an internal control. (b) Supernatants from LPS-stimulated peritoneal macrophages isolated from SIK3-KO and WT mice were harvested at 4 hr after LPS stimulation. IL-6, TNF- α , and IL-10 production was then analysed by ELISA. (c) Supernatants from LPS-stimulated peritoneal macrophages isolated from SIK3-KO and WT mice were harvested at 24 hr after LPS stimulation. NO production was analysed by using Griess reagent. (d) Adenovirus-mediated supplementation of SIK3-WT, SIK3-K37M mutant (kinase-inactive), or LacZ in SIK3-KO or WT TEPM. Western blotting confirmed SIK3 protein over-expression. (e) Culture media from the TEPM that had been infected with adenoviruses (LacZ, SIK3-WT or SIK3-K37M) were harvested for IL-6 measurement at 4 hr after LPS stimulation. (f) SIK3 deficiency did not affect the MyD88-dependent Toll-like receptor 4 (TLR4) -signalling pathway. Thioglycollate-elicited peritoneal macrophages isolated from SIK3-KO or WT mice were harvested at the indicated time-points after LPS stimulation. Western blotting was performed using the indicated antibodies (listed in Materials and methods). α / β -Tubulin was used as an internal control. (g) SIK3 deficiency did not affect the MyD88-independent TLR4-signalling pathway. β -Actin was used as an internal control. The data are expressed as mean \pm SEM ($n = 3$). Statistical analyses were performed using two-way analysis of variance followed by Bonferroni's post-tests (a) or the Student's t -test (b, e) for the comparison of gene expression and cytokine secretion, respectively. * $P < 0.05$, ** $P < 0.01$, *** $P < 0.01$.